Thermoelectric probe for Fermi surface topology in the three-dimensional Rashba semiconductor BiTeI

T. Ideue,[1] L. Ye,[2] J. G. Checkelsky,[2] H. Murakawa,[3] Y. Kaneko,[4] and Y. Tokura[1,4]
[1]*Department of Applied Physics, University of Tokyo, Tokyo 113-8656, Japan*
[2]*Department of Physics, Massachusetts Institute of Technology, Cambridge, Massachusetts 02139, USA*
[3]*Department of Physics, Osaka University, Toyonaka, Osaka 560-0043, Japan*
[4]*RIKEN Center for Emergent Matter Science (CEMS), Wako, Saitama 351-0198, Japan*
(Received 6 June 2015; published 23 September 2015)

We have investigated thermoelectric properties of a three-dimensional Rashba system BiTeI. Magnetic-field dependences of the Seebeck effect and Nernst effect show qualitative changes with the Fermi level passing through the bulk Dirac point, indicating that thermoelectric effects can be a good experimental probe for the Fermi surface topology. The quantum oscillations are observed in the thermoelectric effect of BiTeI under a magnetic field, which are also dependent on the Fermi-level positions and consistent with the energy derivative of the three-dimensional density of states in the Rashba system.

DOI: 10.1103/PhysRevB.92.115144 PACS number(s): 72.20.Pa, 71.20.−b, 71.70.Di, 71.70.Ej

Emergence of exotic electronic band structures by strong spin-orbit interaction (SOI) is of great interest in condensed-matter physics. In systems without inversion symmetry, a SOI-driven effective magnetic field causes the spin splitting in the electronic band structure except at the high-symmetry points in the Brillouin zone, generating the peculiar spin-polarized linear band dispersion. Among them, the Rashba-type SOI [1] in a polar system generates a spin-polarized Dirac fermion; a SOI-induced k-dependent Zeeman field perpendicular to the polar axis and crystal momentum give rise to the chiral spin texture of the electronic band. The Rashba effect has been conventionally studied at the surface [2–4] and interface [5], but recently, a bulk polar semiconductor BiTeI has been proven to host the large Rashba-type SOI [6]. The Rashba-type band structure is unique in the sense that a small inner Fermi surface (IFS) with a spin-polarized Dirac fermion is buried in the large outer Fermi surface (OFS) also with the chiral spin texture. Transport properties originating from the Rashba-type band structure have been reported in the previous studies, such as the characteristic Shubnikov–de Haas (SdH) oscillations [7–12] and magnetophotocurrent measurement [13].

A recent systematic study of SdH oscillations in BiTeI [11] could capture the signature of the Fermi surface topology change. With increasing the mobility and varying the carrier density by Cu doping (see also Ref. [12]) the SdH oscillations were observed for the crystals with different Fermi-level positions. An observed qualitative difference of the SdH oscillations between $E_F \geqslant E_D$ and $E_F \leqslant E_D$ was explained by the scattering process reflecting the three-dimensional (3D) density of sates (DOS) of the IFS in this bulk Rashba system. The purpose of this study is to investigate thermoelectric response (Seebeck and Nernst effects) under a magnetic field in BiTeI with the Fermi level varied around the Dirac point.

Thermoelectric effects have been known as a sensitive experimental tool for probing the electronic states in solids, although they are still less understood theoretically. Quantum oscillations in the thermoelectric effects, for example, were used to study the Landau levels of the electronic band structures in Bi [14,15], graphene [16,17], graphite [18], and various topological insulators [19–21]. The anomaly in the quantum limit [16,17] or during the Fermi surface topology change [18,21] has been discussed in previous works. In this study, we clarified that magnetic-field dependence of the thermoelectric effects is extremely sensitive to the Fermi-level position, reflecting the Fermi surface topology change. In addition, comparative studies of the quantum oscillations in ρ_{xx} (resistivity), S_{xx}, and S_{yx} (longitudinal and transverse thermoelectric coefficients, respectively) give us a further understanding of exotic transport properties and characteristic Landau-level spectra in this system.

Single crystals of BiTeI with high carrier mobility were prepared by the Bridgman method as described in Ref. [11]. Electric and thermoelectric properties were measured with the use of the physical property measurement system (Quantum Design, Inc.). A magnetic field was applied along the c axis, and measurements were performed in magnetic fields up to 14 T. We used a 1-kΩ resistor as the heater, and the temperature difference was measured by type E thermocouples.

Fermi levels (E_F) of the samples cover a wide range of energy including the Dirac point (E_D) of the Rashba-type band structure. Starting from the sample with the lowest Fermi energy, the samples are termed 1–4 as shown in Fig. 1(a). Judging from the carrier concentrations and periods of quantum oscillations, the Fermi levels of sample 1 (with the carrier density $n = 4.6 \times 10^{18}$ cm^{-3} and mobility $\mu = 1.3 \times 10^3$ cm^2 V^{-1} s^{-1}) and sample 2 ($n = 8.3 \times 10^{18}$ cm^{-3}, $\mu = 1.3 \times 10^3$ cm^2 V^{-1} s^{-1}) are assigned to locate below the Dirac point whereas those of sample 3 ($n = 4.2 \times 10^{19}$ cm^{-3}, $\mu = 1.3 \times 10^3$ cm^2 V^{-1} s^{-1}) and sample 4 ($n = 6.7 \times 10^{19}$ cm^{-3}, $\mu = 1.1 \times 10^3$ cm^2 V^{-1} s^{-1}) above E_D as shown in Fig. 1(a). Figures 1(b)–1(d) show the magnetic-field dependences of resistivity, the Seebeck coefficient, and the Nernst signal at $T = 2$ K for each sample. (Transport properties at high temperatures are discussed in the Supplemental Material [22]. From those, we can conclude the negligible effect of phonon drag in the thermoelectric transport [23].) It is to be noticed that magnetic-field dependences of the thermoelectric effects are qualitatively different between

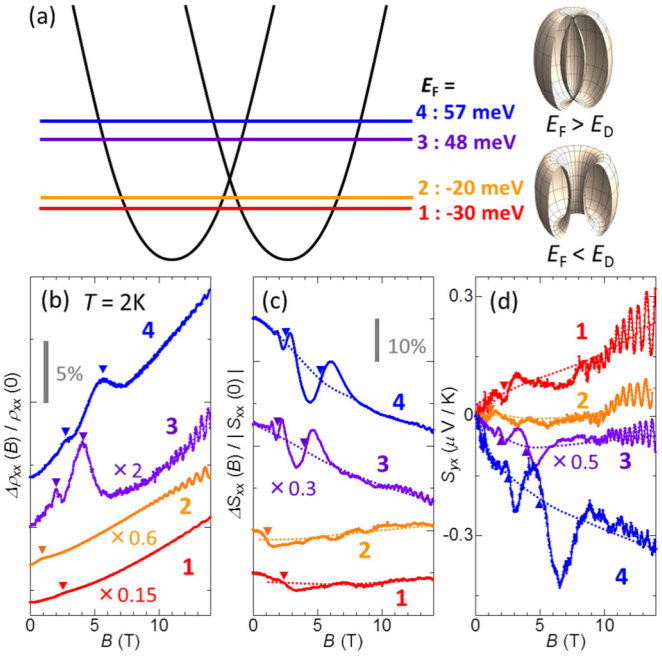

FIG. 1. (Color online) (a) Expected Fermi levels of the measured samples 1–4 and Fermi surface topology for $E_F \geqslant E_D$ and $E_F \leqslant E_D$. The origin of the Fermi level (E_F) is taken at the Dirac point energy (E_D). (b)–(d) Transport properties at $T = 2$ K. Magnetic-field dependences of (b) resistivity, (c) the Seebeck effect, and (d) the Nernst effect. Magnetic-field dependences of S_{xx} and S_{yx} show the qualitative difference between $E_F \geqslant E_D$ and $E_F \leqslant E_D$, whereas ρ_{xx} similarly increases with B. The triangle marks denote the positions of the ρ_{xx} maxima.

$E_F \geqslant E_D$ and $E_F \leqslant E_D$, whereas the magnetoresistivity similarly increases with the magnetic field. S_{xx} of sample 1 and sample 2 show a slight increase with magnetic field B, whereas S_{xx} decreases with B in sample 3 and sample 4. Furthermore, the sign of the Nernst signal is reversed from positive to negative between sample 2 and sample 3. Since the Dirac point lies between Fermi levels of sample 2 and sample 3 [Fig. 1(a)], these differences in S_{xx} and S_{yx} indicate strong sensitivity of the thermoelectric effects to a small IFS pocket and Fermi surface topology. The thermoelectric coefficients are generally related to the Peltier conductivity tensors $\boldsymbol{\alpha}$ as

$$S_{xx} = \rho_{xx}\alpha_{xx} + \rho_{yx}\alpha_{xy}, \tag{1}$$

$$S_{yx} = \rho_{xx}\alpha_{xy} - \rho_{yx}\alpha_{xx}. \tag{2}$$

In the semiclassical regime, Peltier conductivity tensors measure the change in conductivity tensors $\boldsymbol{\sigma}$ by a small chemical potential shift via Mott's relation,

$$\boldsymbol{\alpha} = -\frac{\pi^2}{3}\frac{k_B^2 T}{e}\left(\frac{\partial \boldsymbol{\sigma}}{\partial E}\right)_{E=E_F}, \tag{3}$$

and the Nernst coefficient can be written as the derivative of the Hall angle,

$$S_{yx} = \frac{\pi^2}{3}\frac{k_B^2 T}{e}\frac{\partial}{\partial E}\left[\arctan\left(-\frac{\rho_{yx}}{\rho_{xx}}\right)\right]_{E=E_F}. \tag{4}$$

The contribution of the large OFS to the thermoelectric effect is expected to be small due to the moderate DOS change in BiTeI. By contrast, an anomaly around the IFS Dirac point is much more pronounced in thermoelectric properties than in the resistivity, reflecting the difference of the Fermi surface topology; the IFS area decreases (increases) with E_F below (above) the Dirac point, which causes the increase (decrease) in the Hall angle $-\rho_{yx}/\rho_{xx}$, thus leading to the positive (negative) S_{yx}. It is noteworthy that a similar sign change in the Nernst effect has been also reported for a topological crystalline insulator $Pb_{0.77}Sn_{0.23}Se$ [21]. $Pb_{0.77}Sn_{0.23}Se$ undergoes a topological phase transition and enters into the topological crystalline insulator phase at $T = 180$ K; the Nernst signal shows the sign change around the topological transition temperature although the sign of the Hall effect and Seebeck effect are unaffected. The striking resemblance of the situations between BiTeI and $Pb_{0.77}Sn_{0.23}Se$ implies that similar transitions of Fermi surface topology are realized in both systems [24].

In addition to the semiclassical background signals discussed above, clear quantum oscillations have been observed in all the magnetotransport phenomena at low temperatures. As examined in a previous work [11], the Fermi wave numbers (k_{IFS},k_{OFS}) calculated from the oscillation periods are on the different lines on the k_{IFS} vs k_{OFS} plane, depending on the E_F positions [Fig. 2(a)], which justifies the estimation of the Fermi levels in Fig. 1(a). Furthermore, behaviors of the quantum oscillations are also different between the cases $E_F \geqslant E_D$ and $E_F \leqslant E_D$. ρ_{xx} shows a distinct behavior above

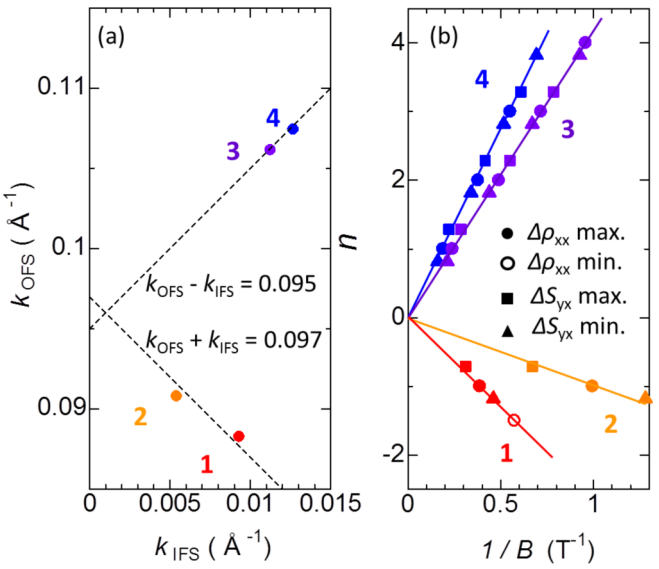

FIG. 2. (Color online) (a) (k_{OFS},k_{IFS}) plots for each sample. k_{OFS} and k_{IFS} stand for the Fermi wavelength for the OFS and IFS, respectively. Points of (k_{OFS},k_{IFS}) are on the line of $k_{OFS} + k_{IFS} = 0.097$ for sample 1 and sample 2 ($E_F \leqslant E_D$), whereas the points of sample 3 and sample 4 ($E_F \geqslant E_D$) are on the different line of $k_{OFS} - k_{IFS} = 0.095$. (b) Landau index plots for the measured samples. The order in the S_{yx} maxima (squares), ρ_{xx} maxima (solid circles), and S_{yx} minima (triangles) is inverted between $E_F \geqslant E_D$ and $E_F \leqslant E_D$. The interval in $1/B$ between the S_{yx} maximum and the ρ_{xx} maximum is not equivalent to that between the S_{yx} minimum and the ρ_{xx} maximum.

the quantum limit, a rapid increase for the sample with $E_F \geqslant E_D$, or suppression in the case of $E_F \leqslant E_D$, which is in accord with the previous work [11]. According to the former analysis [11], such a difference reflects the three-dimensional DOS of the IFS Landau levels in the bulk Rashba system.

As the interpretation of SdH oscillations is well established by previous works [7,11], we analyzed the phase (maximum or minimum positions) of the quantum oscillations in S_{xx} and S_{yx} with respect to the ρ_{xx} oscillations. In Figs. 1(b)–1(d), we marked the B values (triangles) at which ρ_{xx} shows the oscillation peaks corresponding to the DOS maxima of the Landau levels. The ρ_{xx} peaks correspond to the inflection points of the quantum oscillations in S_{xx} and S_{yx} for all samples as shown in Figs. 1(c) and 1(d). However, the phases of these oscillations are different by $\pi/2$ or $-\pi/2$ from those of ρ_{xx} depending on the E_F positions; whether S_{xx} and S_{yx} increase or decrease with B after passing the ρ_{xx} peak points is opposite between $E_F \geqslant E_D$ and $E_F \leqslant E_D$. This can be more clearly seen in the oscillatory components of ρ_{xx}, S_{xx}, and S_{yx} calculated by subtracting the polynomial background [Figs. 3(a) and 3(b)]. In addition, oscillatory components of the thermoelectric coefficients deviate from the ideal sine curve as a function of $1/B$; the widths of the maxima are not equivalent to those of the minima in S_{xx} and S_{yx}. The phase inversion and distortion of the oscillatory components can be also seen in the Landau index plots [Fig. 2(b)]. In these plots, we assigned the ρ_{xx} peak positions (solid circles) to the integer indices following the previous works [7,11] and the points of the S_{yx} maximum (squares) or the S_{yx} minimum (triangles) are shifted so that all points are on the lines determined by the ρ_{xx} plots. The S_{yx} maximum and minimum are assigned to $n \mp 0.28$ and $n \pm 0.18$, respectively, where n is the integer associated with the ρ_{xx} maximum and the signs of $\mp$ and $\pm$ can be determined by the relative position between E_F and E_D ($n - 0.28$ and $n + 0.18$ for $E_F \leqslant E_D$, whereas $n + 0.28$ and $n - 0.18$ for $E_F \geqslant E_D$). Since the oscillatory components in S_{xx} and S_{yx} are similar in shape apart from the sign ($\Delta S_{xx} \propto -\Delta S_{yx}$), we focus here only on the ΔS_{yx} in the Landau index plots. The order in the triangle, circle, and square points in Fig. 2(b), i.e., the sign of $\mp$ or $\pm$ in the above argument, is inverted between $E_F \geqslant E_D$ and $E_F \leqslant E_D$.

The observed phase shift and distortion of the quantum oscillations in the thermoelectric effects can be interpreted in terms of the energy derivative of the three-dimensional DOS of the IFS Landau levels as follows. We show the schematics of the three-dimensional DOS of the IFS Landau levels [$D(E)$] and its energy derivative [$-dD(E)/dE$] in Fig. 3(c). Note that the DOS has the longer tail toward higher energy due to the three-dimensional dispersion which breaks the particle-hole symmetry even around the IFS. As already proven by a previous study [11], resistivity traces the $D(E)$ and reaches extrema when the Fermi level E_F is just at the DOS peak position. At that time, $-dD(E)/dE$ is on the inflection point, which is consistent with the observed oscillations in the thermoelectric effects. In increasing the magnetic field, Landau-level splitting becomes larger, and only low index Landau levels ($n = 0, \pm 1$) dominate the DOS at E_F, which causes the steep decrease (gradual increase) in $-dD(E)/dE$ in the case of $E_F \geqslant E_D$ ($E_F \leqslant E_D$); this is in accord with the

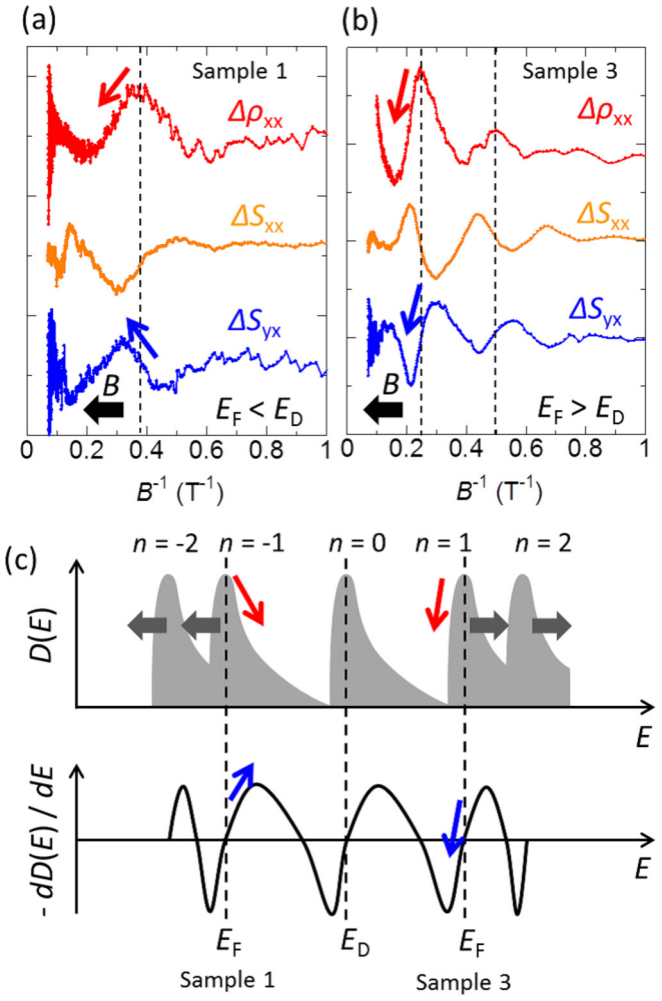

FIG. 3. (Color online) (a) and (b) Oscillating components of the IFS quantum oscillations in (a) sample 1 ($E_F \leqslant E_D$) and (b) sample 3 ($E_F \geqslant E_D$). (c) Schematics of the three-dimensional DOS [$D(E)$] of the IFS Landau level and its energy derivative [$-dD(E)/dE$]. Landau-level splitting becomes larger with increasing magnetic field which makes the Fermi level relatively close to the $n = 0$ Landau level. Accordingly, $\Delta\rho_{xx}$ and ΔS_{yx} trace $D(E)$ and its energy derivative $-dD(E)/dE$, respectively. Due to the three-dimensional dispersion, the DOS has the longer tail toward high energy so that the curve of $-dD(E)/dE$ is distorted.

observation for S_{yx}. Thus, the phase difference of the quantum oscillations between $E_F \geqslant E_D$ and $E_F \leqslant E_D$ or the distortion of the oscillations is considered to reflect the energy derivative of the three-dimensional DOS and hence to be the unique features of the quantum oscillations in the 3D Rashba system. In fact, the Hall angle in Eq. (4) follows the change in ρ_{xx} in the lowest order, thus corresponding to $-D(E)$, which is consistent with the above argument.

Finally, we discuss the difference between the quantum oscillations of the IFS and those of the OFS. In Fig. 4, quantum oscillations in ρ_{xx}, σ_{xx}, S_{yx}, α_{xx}, and α_{xy} for each Fermi surface are shown. The conductivity tensor σ_{xx} is calculated by

$$\sigma_{xx} = \frac{\rho_{xx}}{\rho_{xx}^2 + \rho_{yx}^2}. \quad (5)$$

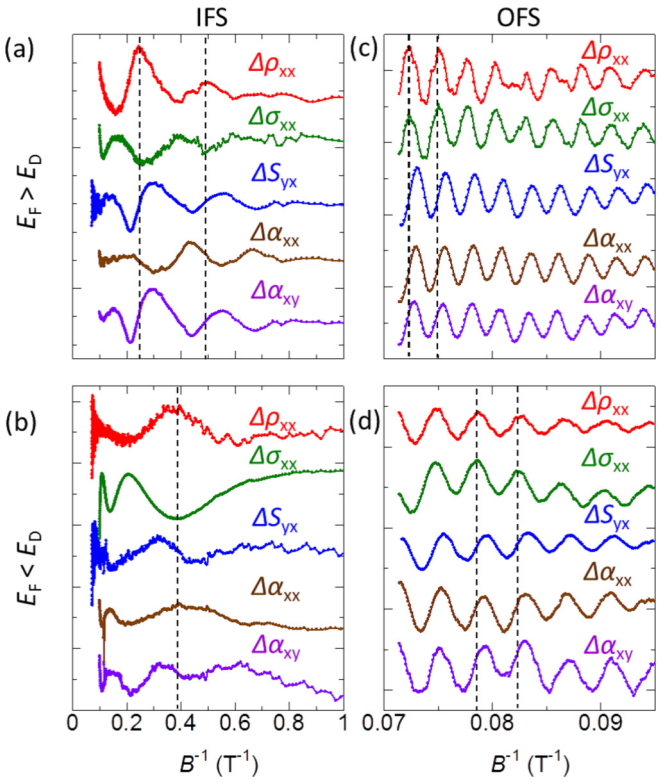

FIG. 4. (Color online) (a)–(d) Oscillatory components of the transport coefficients for (a) and (c) sample 3 ($E_F \geqslant E_D$) and (b) and (d) sample 1 ($E_F \leqslant E_D$). (a) and (b) For the IFS oscillations, the sign of $\Delta\rho_{xx}$ and $\Delta\sigma_{xx}$ is opposite, and the phase of ΔS_{yx} is different by $\pi/2$ or $-\pi/2$ from those of ρ_{xx} depending on $E_F \geqslant E_D$ and $E_F \leqslant E_D$. The contribution from $\Delta\alpha_{xy}$ is dominant in ΔS_{yx}. (c) and (d) For the OFS oscillations, $\Delta\rho_{xx}$ and $\Delta\sigma_{xx}$ are in phase, and the phases of ΔS_{yx} with respect to $\Delta\rho_{xx}$ are the same between $E_F \geqslant E_D$ and $E_F \leqslant E_D$.

In the low magnetic-field region, the Hall angle is small ($|\rho_{yx}/\rho_{xx}| \ll 1$) so that the phases of $\Delta\rho_{xx}$ and $\Delta\sigma_{xx}$ are opposite ($\Delta\rho_{xx} \propto -\Delta\sigma_{xx}$) and the $\Delta\alpha_{xy}$ term is dominant in ΔS_{yx} ($\Delta S_{yx} \propto \Delta\alpha_{xy}$) [Figs. 4(a) and 4(b)]. As we assigned the ρ_{xx} maximum to the DOS peak, the opposite phase in ρ_{xx} and σ_{xx} indicates the scattering nature of the IFS oscillations; the carriers of the OFS which dominate in the electric charge transport are scattered by the IFS carriers so that the decrease in σ_{xx} (increase in ρ_{xx}) can be attributed to the DOS of the IFS. On the other hand, the Hall angle becomes large in the high magnetic-field region, which leads to the same phase of the oscillations in ρ_{xx} and σ_{xx} ($\Delta\rho_{xx} \propto \Delta\sigma_{xx}$). Because the oscillatory components in S_{yx} are large, both α_{xx} and α_{xy} calculated by Eqs. (1) and (2) show the similar oscillatory components [Figs. 4(c) and 4(d)]. There are no more oscillatory features associated with IFS Landau levels in this regime. The phase inversion between $E_F \geqslant E_D$ and $E_F \leqslant E_D$ observed for the IFS thermoelectric oscillations is no longer discernible in the OFS oscillations, indicating the lack of anomaly for the OFS DOS around the IFS Dirac point as expected.

To summarize, we have found that thermoelectric properties of BiTeI critically depend on the Fermi-level positions. Magnetic-field dependence of the Seebeck effect and the sign of the Nernst signal change in the vicinity of the Dirac point, reflecting the Fermi surface topology change. By the comparative studies of quantum oscillations in electric and thermoelectric properties, we showed that the phase difference between $E_F \geqslant E_D$ and $E_F \leqslant E_D$ as well as the distortion of the quantum oscillations in thermoelectric effects can be explained by the energy derivative of the three-dimensional DOS in the Rashba spin-splitting conduction bands.

The authors thank M. S. Baharamy, N. Nagaosa, and N. Kanawzawa for fruitful discussions. This work was supported by Grants-in-Aid for Scientific Research (S) (Grant No. 24224009) from the Ministry of Education, Culture, Sports, Science and Technology (MEXT) of Japan and the Funding Program for World-Leading Innovative R&D on Science and Technology (FIRST Program) on "Quantum Science on Strong Correlation" initiated by the Council for Science and Technology Policy, Japan.

[1] E. I. Rashba, Sov. Phys. Solid State **2**, 1109 (1960).
[2] S. LaShell, B. A. McDougall, and E. Jensen, Phys. Rev. Lett. **77**, 3419 (1996).
[3] C. R. Ast, J. Henk, A. Ernst, L. Moreschini, M. C. Falub, D. Pacilé, P. Bruno, K. Kern, and M. Grioni, Phys. Rev. Lett. **98**, 186807 (2007).
[4] Y. M. Koroteev, G. Bihlmayer, J. E. Gayone, E. V. Chulkov, S. Blügel, P. M. Echenique, and P. Hofmann, Phys. Rev. Lett. **93**, 046403 (2004).
[5] J. Nitta, T. Akazaki, H. Takayanagi, and T. Enoki, Phys. Rev. Lett. **78**, 1335 (1997).
[6] K. Ishizaka, M. S. Bahramy, H. Murakawa, M. Sakano, T. Shimojima, T. Sonobe, K. Koizumi, S. Shin, H. Miyahara, A. Kimura, K. Miyamoto, T. Okuda, H. Namatame, M. Taniguchi, R. Arita, N. Nagaosa, K. Kobayashi, Y. Murakami, R. Kumai, Y. Kaneko, Y. Onose, and Y. Tokura, Nature Mater. **10**, 521 (2011).
[7] H. Murakawa, M. S. Bahramy, M. Tokunaga, Y. Kohama, C. Bell, Y. Kaneko, N. Nagaosa, H. Y. Hwang, and Y. Tokura, Science **342**, 1490 (2013).
[8] C. Bell, M. S. Bahramy, H. Murakawa, J. G. Checkelsky, R. Arita, Y. Kaneko, Y. Onose, M. Tokunaga, Y. Kohama, N. Nagaosa, Y. Tokura, and H. Y. Hwang, Phys. Rev. B **87**, 081109(R) (2013).
[9] C. Martin, E. D. Mun, H. Berger, V. S. Zapf, and D. B. Tanner, Phys. Rev. B **87**, 041104(R) (2013).
[10] T. Ideue, J. G. Checkelsky, M. S. Bahramy, H. Murakawa, Y. Kaneko, N. Nagaosa, and Y. Tokura, Phys. Rev. B **90**, 161107(R) (2014).
[11] L. Ye, J. G. Checkelsky, F. Kagawa, and Y. Tokura, Phys. Rev. B **91**, 201104(R) (2015).
[12] C. R. Wang, J. C. Tung, R. Sankar, C. T. Hsieh, Y. Y. Chien, G. Y. Guo, F. C. Chou, and W. L. Lee, Phys. Rev. B **88**, 081104(R) (2013).
[13] N. Ogawa, M. S. Bahramy, H. Murakawa, Y. Kaneko, and Y. Tokura, Phys. Rev. B **88**, 035130 (2013).
[14] K. Behnia, M. A. Méasson, and Y. Kopelevich, Phys. Rev. Lett. **98**, 166602 (2007).
[15] K. Behnia, L. Balicas, and Y. Kopelevich, Science **317**, 1729 (2007).

[16] Y. M. Zuev, W. Chang, and P. Kim, Phys. Rev. Lett. **102**, 096807 (2009).

[17] J. G. Checkelsky and N. P. Ong, Phys. Rev. B **80**, 081413(R) (2009).

[18] Z. Zhu, H. Yang, B. Fauqué, Y. Kopelevich, and K. Behnia, Nat. Phys. **6**, 26 (2010).

[19] D. X. Qu, Y. S. Hor, and R. J. Cava, Phys. Rev. Lett. **109**, 246602 (2012).

[20] B. Fauqué, N. P. Butch, P. Syers, J. Paglione, S. Wiedmann, A. Collaudin, B. Grena, U. Zeitler, and K. Behnia, Phys. Rev. B **87**, 035133 (2013).

[21] T. Liang, Q. Gibson, J. Xiong, M. Hirschberger, S. P. Koduvayur, R. J. Cava, and N. P. Ong, Nat. Commun. **4**, 2696 (2013).

[22] See Supplemental Material at http://link.aps.org/supplemental/10.1103/PhysRevB.92.115144 for the temperature dependence of the Nernst effect and quantum oscillations.

[23] Effect of phonon drag in the Nernst signal of Bi was discussed in V. N. Galev, V. A. Kozlov, N. V. Kolomoets, S. Y. Skipidarov, and N. A. Tsvetkova, JETP Lett. **33**, 106 (1981); M. Matsuo, A. Endo, N. Hatano, H. Nakamura, R. Shirasaki, and K. Sugihara, Phys. Rev. B **80**, 075313 (2009).

[24] Indeed, the authors of Ref. [21] discussed the similarity of the Fermi surface topology between BiTeI and $Pb_{0.77}Sn_{0.23}Se$ (possible existence of a small Fermi surface pocket surrounded by a larger Fermi surface).